Springer

Journal of
Mechanical
Science and
Technology

Journal of Mechanical Science and Technology 22 (2008) 1019~1029

www.springerlink.com/content/1738-494x

An investigation of higher-order closures in the computation of the flow around a generic car

Yong-Jun Jang*

Aerodynamic Research Team, Track & Civil Engineering Research Department, Korea Railroad Research Institute
#360-1, Woulam-Dong, Uiwang-City, Kyounggi-Do, Korea, 437-757

(Manuscript Received November 6, 2007; Revised January 17, 2008; Accepted February 4, 2008)

Abstract

The ability of non-linear eddy-viscosity and second-model-closure models to predict the flow around a simplified three-dimensional car body, known as the "Ahmed body," is investigated with a steady RANS scheme. The principal challenge is to predict the separation from and reattachment onto the slanted rear roof portion at the slant angle 25°, which is close to the critical value at which separation is just provoked from the roof surface. At these conditions, it has been conjectured that separation is intermittent, with periodic flapping being a highly influential process. This is thus an exceptionally challenging case, especially for low-Re models, as the geometrical complexity occurs together with high-Re conditions (Re = 768,000) and highly complex flow features in the wake of the body. A 1.89M-node mesh containing 44-blocks was employed for one half of the spanwise symmetric body. The results demonstrate that the Reynolds-stress-transport model employed is able to reproduce, in contrast to all other models, the reattachment of the flow on the slanted rear surface. As a consequence, the strong streamwise vortices emanating from the sides of the body and associated with lift and circulation are also reproduced in good agreement with experimental data. The physical processes at play and the reasons for the predictive differences are discussed.

Keywords: Turbulence; Separation; Non-linear eddy-viscosity modelling; Reynolds-stress modelling

1. Introduction

The shape of most car bodies is an intermediate between a bluff and a streamlined body. While streamlining is a crucial feature of such bodies, bluntness cannot be avoided because of the relatively large height-to-length ratio that goes with the need to provide for a roomy inside cavity. Thus, almost all car bodies provoke significant separation at the rear and a recirculating wake, which are major contributors to the drag on the vehicle. One important issue affecting the drag as well as the lift is the state of flow over the rear slanted window surface that bridges the roof with the rear end. If the slant angle is sufficiently large, the flow separates from the roof; otherwise it is attached. The critical angle separating the two states is thus of much interest. There is no unique angle, of course, because the state of the flow over the slanted portion depends greatly on the shape of other parts of the car body as well as on the curvature of the 'corner' linking the slanted surface with the roof. The trend towards virtual-car design clearly implies the need to be able to predict the above interaction, because of its major impact on the car's aerodynamic performance.

The approach on which industry relies in the large majority of circumstances is based on the solution of the Reynolds-averaged Navier-Stokes equations in conjunction with turbulence models. While there have been recent efforts to apply large eddy simulation to generic car bodies (Hinterberger et al. [1], Krajnovic and Davidson [2]), these are fraught with difficulties that arise from the extremely high resource requirements at the high Reynolds numbers involved, and

*Corresponding author. Tel.: +82 31 460 5355, Fax.: +82 31 460 5319
E-mail address: jangyj@krri.re.kr
DOI 10.1007/s12206-008-0205-3

the highly constraining grid requirements, especially close to the wall. This is certainly not an approach that is likely to be adopted in practice for some time to come. The alternative of applying unsteady RANS may hold some promise, because of the likely impact of the dynamics of the large-scale energetic motions in massive separation, but this approach relies on the presence of a strong flow instability, usually in the form of periodic shedding. Such shedding may be present in the wake of bluff bodies, but the separation process from streamlined portions, such as the slanted rear window area, is not necessarily one that falls into this category.

Against the above background, the question of what can be achieved in the computation of separated road-vehicle flows by the use of advanced turbulence closures, within a steady-state RANS framework, remains a topic of substantial interest. This topic is the focus of the present paper. The opportunity to address this question has arisen with extensive and well-regarded experimental data being generated by Lienhart and Becker [3] for the so-called *Ahmed Body* (Ahmed et al. [4]), shown in Fig. 1. A particular issue addressed in the experiments is the dependence of the separation from the roof/rear-window corner on the slant angle. Measurements were made to two angles, 25^o and 35^o. In the latter case, the flow is fully detached, and the modelling challenge is relatively modest. At an angle of 25^o, the experiments indicate a time-mean behaviour which is characterized by separation from the roof-window corner and reattachment on the slanted surface. Hence, this angle must be close to the critical value that separates the states of attached from separated flow, and this is not only the most challenging case to compute, but also the most interesting from a practical as well as fundamental point of view.

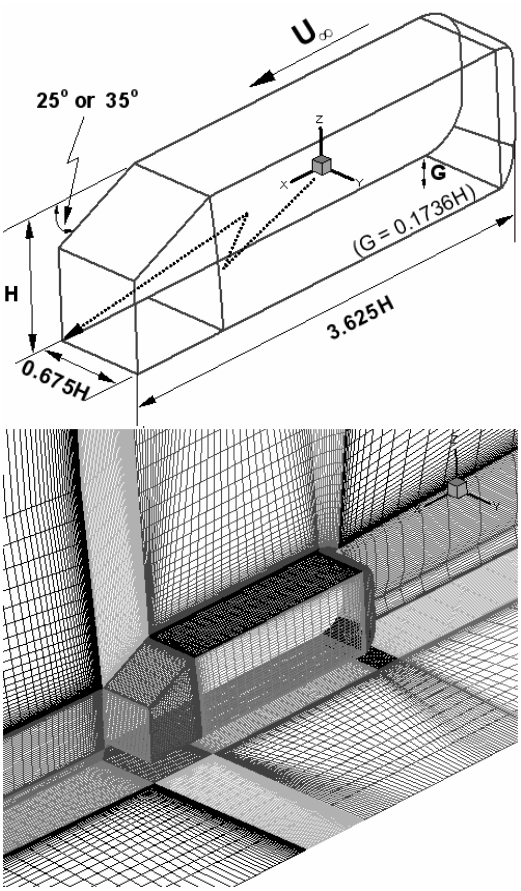

Fig. 1. Car-body geometry and mesh.

In the present computational study, low-Reynolds-number forms of non-linear eddy-viscosity and second-moment closure are applied to half the body with symmetry assumed, the target being a steady mean flow. The computations were undertaken, in part, as a contribution to the 10th ERCOFTAC/IAHR Workshop on Refined Turbulence Modelling (Manceau and Bonnet [5]).

2. Computational representation

The geometry and the grid are shown in Fig. 1. The front face of the body is located at a distance of 7.3H from the channel inlet (H being the body height) and the downstream length between the rear face of the body and channel outlet is 18.12H. The body is elevated above the floor by stilts, producing a ground clearance of 0.174H, the same as in the experiments. However, the stilts supporting the body have not been included in the computational representation. The Reynolds number, based on the incoming velocity U_∞ and car height H, is $Re = 7.68\times10^5$. A uniform velocity profile was used as the inlet boundary condition. The spanwise box extends from the center plane to 3.1H, and symmetry conditions are applied to both spanwise boundaries.

The grid contains 44 blocks and 1.89 million nodes. The computational cells are concentrated where they are mostly needed--in boundary layers and regions of separated flows. This is achieved by using the blocking topology combining O- and C- and H-blocks. The grid-lines in the near-wall block are arranged to be

nearly orthogonal over the most important parts of the body. The distance of the wall-nearest grid layer to the wall is of order y^+=1 over most parts of the body, especially in the rear portion.

Computations were performed with a non-orthogonal, collocated, cell-centered finite-volume approach implemented in the code 'STREAM' (Lien and Leschziner [6], Apsley and Leschziner [7]). Convection of both mean-flow and turbulence quantities was approximated by the 'UMIST' scheme (Lien and Leschziner [8]) - a second-order TVD approximation of the quadratic-interpolation scheme QUICK. Mass conservation was enforced indirectly by way of a pressure-correction algorithm. Within this scheme, the transport and the pressure-correction equations are solved sequentially and iterated to convergence.

3. Turbulence modelling

Computations have been performed with two non-linear eddy-viscosity models of Apsley & Leschziner [9] and Abe et al. [10], respectively, and the Reynolds-stress-transport model of Speziale et al. [11], combined with a low-Re near-wall extension by Chen et al [12]. These are contrasted with results for two linear eddy-viscosity models: the linear low-Re k-ε model of Launder and Sharma [13] and the low-Re k-ω model of Wilcox [14].

While both non-linear eddy-viscosity models (NLEVMs) have been obtained by simplification of algebraic forms of associated Reynolds-stress models, both may be expressed by the following canonical, cubic stress-strain/vorticity constitutive equation:

$$\begin{aligned}\mathbf{a} = &-2C_\mu\mathbf{s} + q_1\left(\mathbf{s}^2 - \frac{1}{3}s_2\mathbf{I}\right) + q_2\left(\mathbf{ws}-\mathbf{sw}\right)\\ &+ q_3\left(\mathbf{w}^2 - \frac{1}{3}w_2\mathbf{I}\right) - \gamma_1 s_2\,\mathbf{s} - \gamma_2 w_2\,\mathbf{s}\\ &- \gamma_3\left(\mathbf{w}^2\mathbf{s} + \mathbf{sw}^2 - w_2\mathbf{s} - \frac{2}{3}\{\mathbf{wsw}\}\mathbf{I}\right)\\ &- \gamma_4\left(\mathbf{ws}^2 - \mathbf{s}^2\mathbf{w}\right) \qquad (1)\end{aligned}$$

in which **a** is the stress anisotropy tensor, **s** is the strain tensor, **w** is the vorticity tensor, $\mathbf{I}=\delta_{ij}$ (Kronecker Delta), $s_2 = -\bar{s}^2/2$, $w_2 = -\bar{w}^2/2$, $\bar{s} = \sqrt{2s_{ij}s_{ij}}$, $\bar{w} = \sqrt{2w_{ij}w_{ij}}$ and the coefficients are model-dependent, but generally functions of $k=\frac{1}{2}\overline{u_iu_i}$ and the dissipation rate ε or the specific dissipation rate $\omega=\varepsilon/k$.

The Apsley and Leschziner model (denoted by AL) is a cubic low-Re k-ε form derived from a simplification of the algebraic Reynolds-stress model of Rodi [15]. Thus, the explicit cubic stress-strain/ vorticity relationship was obtained through a two-step iterative substitution of the implicit algebraic relationships implied by the parent Reynolds-stress model. The model coefficients were then determined as a function of y^* ($=y\sqrt{k}/\nu$) by reference to DNS data for a number of near-wall flows, so as to ensure that the correct normal-stress separation is returned in the near-wall layer. Finally, functional corrections were introduced to account for non-equilibrium conditions $P_k/\varepsilon \neq 1$. In common with the model of Gatski & Speziale [16], the present model also uses $C_{\varepsilon 1}$ = 1.44 and $C_{\varepsilon 2}$ = 1.83 in the ε-equation. This enhances the tendency towards separation in the presence of adverse pressure gradient.

The model by Abe, Jang and Leschziner (denoted by AJL) is a quadratic low-Re model which differs in two important respects from others. First, it augments the basic quadratic form of the constitutive relation in eq. (1) by two additive fragments intended to account, respectively, for high normal straining and strong near-wall anisotropy. Second, the variant used here incorporates a ω-equation that is much closer than Wilcox's form to the ε-equation. Specifically, it includes products of k and ω gradients and coefficients for the production and destruction terms which are directly equivalent to $C_{\varepsilon 1}$ and $C_{\varepsilon 2}$ normally used in the ε-equation. An influential model fragment accounts specifically for strong near-wall anisotropy and for the correct decay towards two-component turbulence that is observed in DNS. This decay cannot be represented solely by the use of terms combining the strain and vorticity. The approach taken by Abe et al. was thus to add a tensorially correct wall-related term to the constitutive stress-strain/vorticity relation $a_{ij} \equiv \frac{\overline{u_iu_j}}{k} - \frac{2}{3}\delta_{ij} = f(\mathbf{s},\mathbf{w}...)$, which takes into account the wall orientation. In the model variant used here, the wall-direction indicator is:

$$d_i = \frac{N_i}{\sqrt{N_kN_k}} \qquad N_i = \frac{\partial l_d}{\partial x_i} \qquad l_d = y_n \text{ (=wall distance)} \quad (2)$$

which is then used in the additive wall-anisotropy correction of the form:

$$ {}^{w}a_{ij} = -f_w\left(d_i d_j - \frac{\delta_{ij}}{3} d_k d_k \right) \times f(\mathbf{s}^2, \mathbf{sw}, \mathbf{ws}, \mathbf{w}^2 s_2, w_2 ...) \tag{3} $$

where f_w is a viscosity-related damping function (see Jang et al. [17] for details). Alternative wall-orientation indicators that are independent of wall distance may readily be used. In the above damping function, a composite time scale is used, which combines the macro-scale k/ε with the Kolmogorov scale $\sqrt{\nu/\varepsilon}$. The damping function f_w then provides a smooth transition between the two scales across the near-wall layer. The model is fully described in Abe et al. [10] and Jang et al. [17], and the latter publication demonstrates, by way of results for the anisotropy and its invariants, that the model indeed returns the correct wall-asymptotic behavior of the stresses for separated flow in a 2-d constricted duct.

The Reynolds-stress-transport model (RSTM) of Speziale, Sarkar and Gatski (denoted by SSG) is applicable, in its original form, to high-Reynolds-number flow only. Here, a low-Re extension by Chen et al. [12] has been adopted to avoid uncertainties associated with wall functions in separated flow. The model solves equations of the form:

$$ \frac{\partial}{\partial t}(\rho \overline{u_i u_j}) + \frac{\partial}{\partial x_k}(\rho U_k \overline{u_i u_j}) = \frac{\partial}{\partial x_k} d_{ijk} + \rho(P_{ij} + \Phi_{ij} - \varepsilon_{ij}) \tag{4} $$

$$ \frac{\partial}{\partial t}(\rho\varepsilon) + \frac{\partial}{\partial x_k}(\rho U_k \varepsilon) = \frac{\partial}{\partial x_k} d_k^{(\varepsilon)} + \rho(C_{\varepsilon 1} f_1 P - C_{\varepsilon 2} f_2 \varepsilon)\frac{\varepsilon}{k} + \rho(S_l + S_\varepsilon) \tag{5} $$

Where

$$ P_{ij} = -(\overline{u_i u_k}\frac{\partial U_j}{\partial x_k} + \overline{u_j u_k}\frac{\partial U_i}{\partial U_k}), \quad P = \frac{1}{2} P_{ii} \tag{6} $$

$$ d_{ijk} = d_{ijk}^{(p)} + d_{ijk}^{(u)} + \mu \frac{\partial}{\partial x_k}(\overline{u_i u_j}) \tag{7} $$

$$ \varepsilon = \frac{1}{2}\varepsilon_{kk} \tag{8} $$

For diffusion

$$ d_{ijk} = (\mu\delta_{kl} + C_s \frac{\rho k \overline{u_k u_l}}{\varepsilon})\frac{\partial}{\partial x_l}(\overline{u_i u_j}) \tag{9} $$

$$ d_k^{(\varepsilon)} = (\mu\delta_{kl} + C_\varepsilon \frac{\rho k \overline{u_k u_l}}{\varepsilon})\frac{\partial \varepsilon}{\partial x_l} \tag{10} $$

$$ C_s = 0.22, \quad C_\varepsilon = 0.18 \tag{11} $$

For pressure strain

$$ \Phi_{ij} = \Phi_{ij}^{(1)} + \Phi_{ij}^{(2)} \tag{12} $$

Where

$$ \Phi_{ij}^{(1)}/\varepsilon = -C_1 \mathbf{a} - C_1^{'}(\mathbf{a}^2 - \frac{1}{3} a_2 \mathbf{I}) \tag{13} $$

$$ \Phi_{ij}^{(2)}/\varepsilon = C_{01}(\mathbf{s} - \frac{1}{3} S_1 \mathbf{I}) + C_{11}(\mathbf{sa} + \mathbf{as} - \frac{2}{3}\{\mathbf{as}\}\mathbf{I}) + C_{12}(\mathbf{wa} - \mathbf{aw}) \tag{14} $$

$$ C_1 = 1.7 + 0.9\frac{P}{\varepsilon}, \quad C_1^{'} = -1.05, \quad C_{01} = 0.8 - 0.65 a_2^{1/2}, \quad C_{11} = 0.625, \quad C_{12} = 0.2 \tag{15} $$

$$ C_{\varepsilon 1} = 1.44, \quad C_{\varepsilon 2} = 1.83 \tag{16} $$

The pressure-strain term, Φ_{ij}, is modelled by a quasi-linear approximation (see Speziale et al. [11]) without a wall-reflection term, the dissipation term is approximated by the isotropic-process form $\varepsilon_{ij} = \frac{2}{3}\varepsilon\delta_{ij}$, the production terms ($P_{ij}$) and the advection terms are exact, and diffusion is approximated by the "generalized gradient-diffusion hypothesis" (GGDH) $d_{ijk} = (\mu\delta_{kl} + C_s \frac{\rho k}{\varepsilon}\overline{u_k u_l})\frac{\partial}{\partial x_l}(\overline{u_i u_j})$. Finally, closure of the system is effected by a ε-equation, which is essentially a variation on the equation used in k-ε eddy-viscosity models. Chen et al.'s [12] extension included the introduction of the damping function $f_w = \exp[-(0.0484\frac{\sqrt{k}y}{\nu})^4]$ into the pressure-strain model, the addition of a wall-related fragment to the pressure-strain model, also weighted by f_w so as to make it vanish at the wall, and a form of the ε-equation, made applicable to low-Re regions by the inclusion of f_w and a second damping function $f_\varepsilon = 1 - \frac{2}{9}\exp[-(R_t/6)^2]$ in which $R_t = \frac{k^2}{\nu\varepsilon}$ represents the viscous effects.

4. Results

Results presented in Figs. 2-5 aim to convey the major elements of and the differences in the performance of the turbulence models investigated, with emphasis being placed on the NLEVMs and the RSTM.

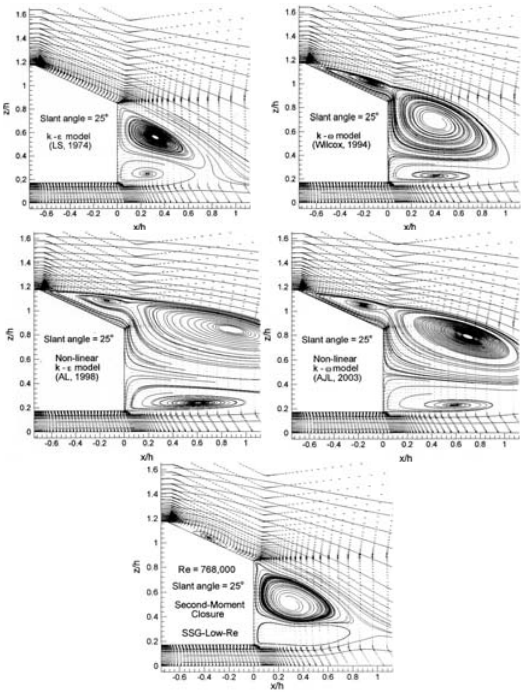

Fig. 2. Stream-traces and velocity vector fields in the body's center-plane.

These results form a modest subset of those assembled and compared with the experimental data; much additional information is available on velocity and turbulence variations upstream and downstream of the body portion containing the slanted surface. However, the data included below suffice to justify the principal conclusions drawn at the end.

From a practical point of view, the parameters of principal interest are the drag and lift. These are affected most strongly by the flow features on the rear of the body, especially the manner in which the flow behaves on the rear slanted surface. It is instructive, therefore, to highlight first the major fluid-mechanic processes which give rise to the observed flow pattern in this region.

Experiments show that the flow on the slanted surface is characterized by two dominant, interacting features: (i) two large streamwise-oriented vortices which separate from the two upper rear corners formed as the junction of the roof, the side walls and the slanted surface, and (ii) by separation from the central portion of the edge formed by the roof and the slanted surface, followed by reattachment on that same surface. At the slant angle considered, the mixing rate in the roof boundary layer is almost sufficient for the boundary layer to resist the adverse pressure gradient caused by the downward slant and to prevent separation from the upper edge. The flow is drawn downwards, therefore, and the strong curvature-induced centripetal body force is compensated by a cross-flow pressure gradient creating suction on the central portion of the slanted surface, much like that occurring on the suction side of a wing. The lift associated with the above process implies a high level of circulation around the body, which has to be shed from the sides of the body, again in analogy to a wing. This shedding occurs through the strong corner vortices noted above, which are analogous to the well-known wing-tip vortices on aeroplanes. Hence, the intensity of these vortices downstream of the separation region is an indication of the lift on the body. Because the suction is highest on the spanwise-central portion of the slanted surface, the separated vortices are drawn towards the center. The rotational orientation in the vortices is such that fluid is preferentially pushed downwards, towards the spanwise ends of the slanted surface, so that the 'quasi-2d' separation observed in the central portion of the surface is prevented at its sides. This highly interactive process thus gives rise to a complex three-dimensional flow pattern on the rear side. The dominant features are thus (i) a quasi-2d separation and reattachment in the (spanwise) central portion of the slanted surface, (ii) 'attached' but highly skewed flow on much of the surface close to the spanwise sides, and (iii) detachment and attachment lines on the slanted surface arising the interaction between the side vortices with the boundary layers emanating from the roof as well as the side walls and the body's underside.

Fig. 2 shows three types of predictive behavior on the spanwise central plane: (i) a fully attached flow on the slanted surface, followed by a short recirculation region, predicted by the linear k-ε model; (ii) a fully detached flow, with very large recirculating wakes, predicted by the linear k-ω and both NLEVMs; and (iii) a detached and reattaching flow with relatively short recirculating wake, predicted by the RSTM. Thus, based purely on the state of the flow on the central plane, only the Reynolds-stress model returns the correct behavior. As seen, the linear k-ε model behaves much as expected, failing to predict separation in circumstances in which the flow is close to the separation/attachment limit. While the linear k-ω model does not comply with this general trend of linear models, this is due to a combination of

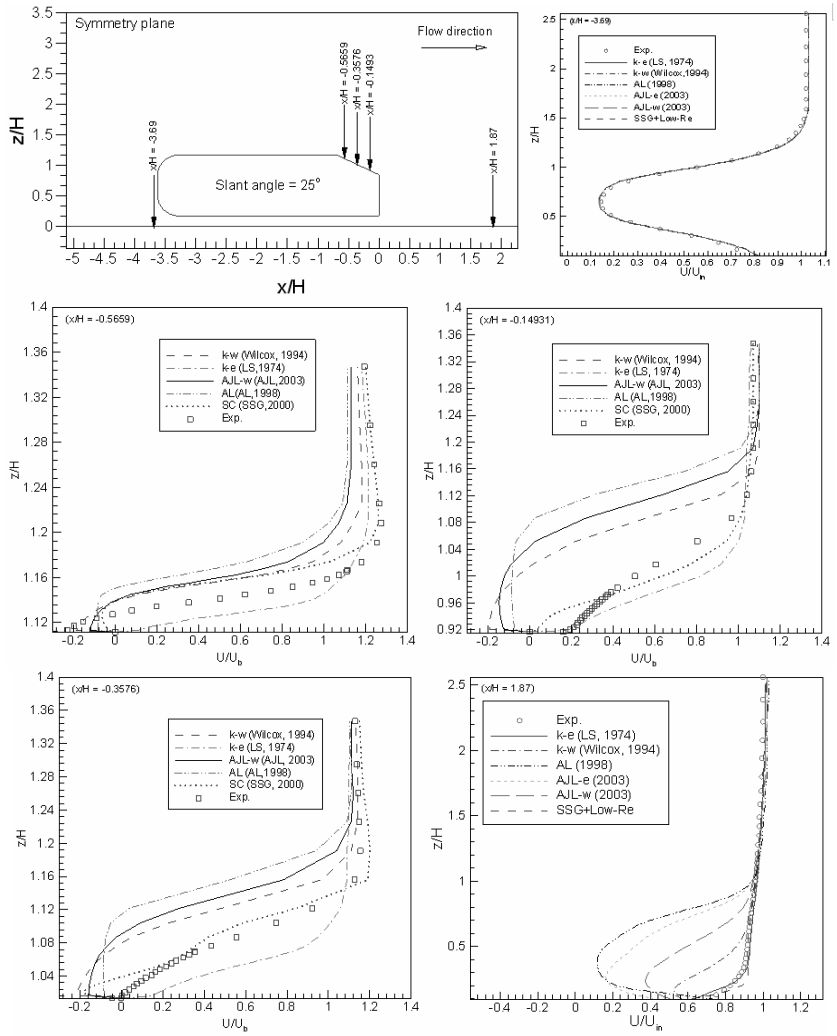

Fig. 3. Streamwise-velocity profiles ahead of the body and above and behind the slanted surface on the body's center-plane.

peculiarities of the ω-equation in the model, the particular choice of constants in this equation and known defects in the viscosity-related damping functions of that low-Re version of the model (for further discussion of these issues, see Apsly and Leschziner [7, 9, 18]). In studies of 2-d flow (Jang et al. [17]), this model is also observed to give a trend towards excessive separation. The fact that the NLEVMs fare poorly is disappointing, but not entirely unexpected. In simple terms, these models aim to counteract the tendency of linear models to predict excessive levels of turbulence and hence mixing, thus inhibiting separation. This is achieved, essentially, by terms that sensitize the turbulence properties, more appropriately than is done by linear models, to curvature, high strain rate and normal straining provoked by impingement and adverse pressure gradient. The study by Jang et al. [17] shows the AJL model to give very satisfactory behavior in 2-d separation from the curved surface of a constriction in a duct, while the AL model was found to significantly over-estimate the extent of the recirculation zone. Here, however, the model fails to reproduce reattachment on the slanted surface, implying insufficient mixing in the separated shear layer. In fact, the study by Jang et al. shows that insufficient turbulence energy and shear stress in the separated shear layer is a defect shared by all nine linear and no-linear EVMs examined in that study. Of these, the AJL model was shown to give the least serious underestimate, however.

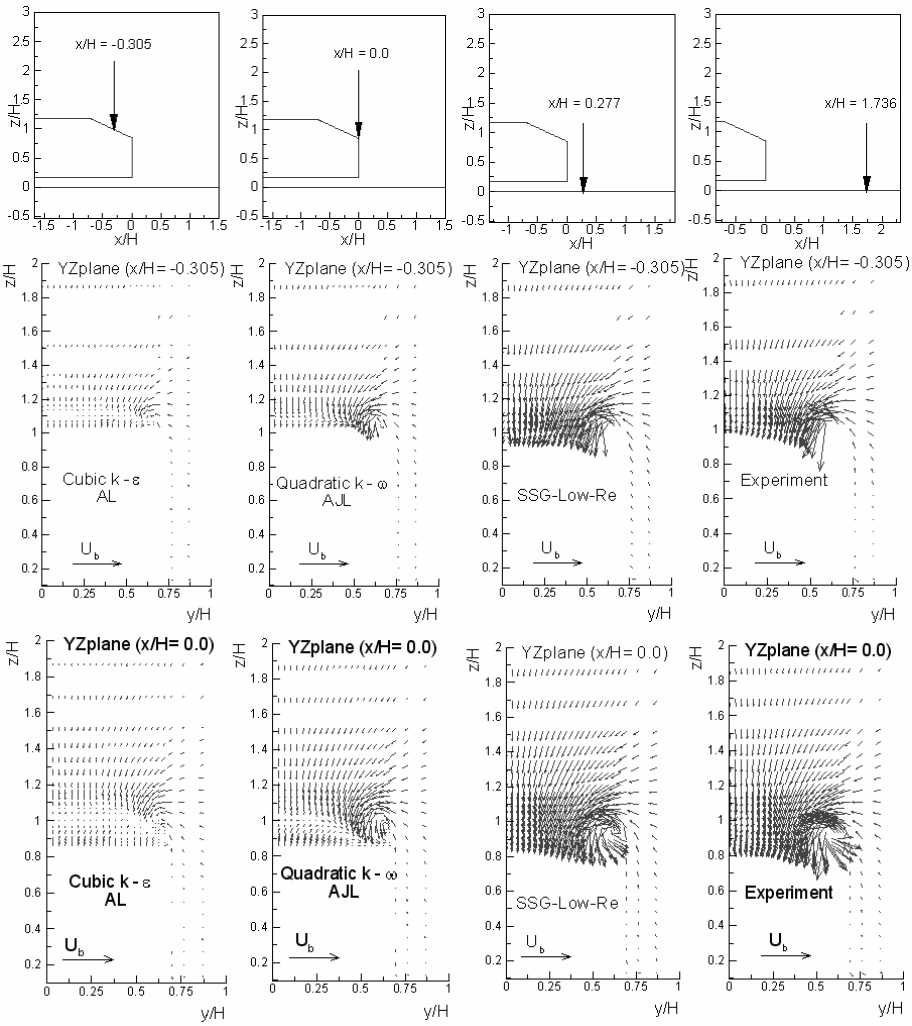

Fig. 4. Transverse-velocity-vector fields in *y-z* planes above the slanted surface and behind the body; streamwise positions of the *y-z* planes shown in top four inserts.

Fig. 3 reinforces the observations made in relation to Fig. 2. This shows velocity profiles on the center-plane at five streamwise stations: one ahead of the body, three above the slanted surface and one in the 'far' wake. The first set of profiles, just upstream of the body, is included to demonstrate that the flow approaching the body is computed correctly and is insensitive to turbulence modelling. While none of the turbulence models may be claimed to give a satisfactory representation of the flow in the rear part of the body, it is seen that the RSTM indeed reproduces the separation from the roof and the reattachment on the slanted surface, whereas the NLEVMs fail to give reattachment and seriously over-estimate the reverse flow, especially the AL model observed in earlier studies, to give a particularly low level of turbulent mixing in curved shear layers. As expected, those models returning the most serious over-estimate of the separation above the slanted surface also give the largest far-wake defect. Only the linear k-ε model and the RSTM give a broadly correct far-wake flow, but it is recalled that the former model fails to capture the separation on the slanted surface.

Given that the flow around the spanwise central portion of the slanted surface is critically important, the expectation is that only the RSTM will give a reasonably adequate representation of the vortices emanating from the upper sides of the body. Fig. 4 confirms this expectation. It shows transverse velocity fields at four streamwise locations, including two in

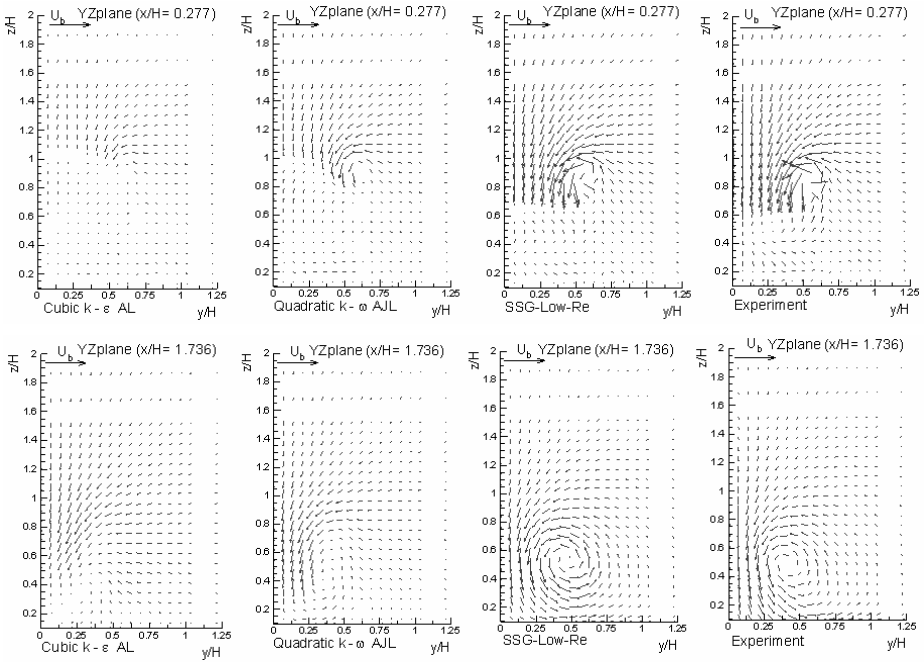

Fig. 4. (continued) Transverse-velocity-vector fields in y-z planes above the slanted surface and behind the body.

the wake behind the body. The correspondence between the RSTM solution and experiment is remarkable. It is important to point out here that the formation and, to some degree, the evolution of the vortices is dictated largely by inviscid mechanisms – specifically the lift and circulation, except in so far as the turbulent processes in the separated shear layer above the slanted surface affect the pressure field and therefore the lift. What Fig. 4 shows, therefore, is that the behavior of the upper separated shear layer is broadly correctly reproduced: the circulation is broadly correct and the strength of the shed vortices is close to reality. In contrast, the flow produced by the NLEVMs in the central region above the slanted surface is wrong, the circulation is too low, and hence the vortices are too weak, especially in the case of the AL model.

The observed failure of most models to predict separation and reattachment has been attributed, tentatively, to the intermittent nature of the separation process, that is, loosely, to an organized 'flapping' of the separated shear layer. This explanation arises from the observation that the measured turbulence level in the separated shear layer above the slanted surface was much higher than that computed by all models, the consequences being a substantial 'turbulence' contribution from the organized component. As this process cannot be resolved by any steady RANS computation, the expectation was that no model would successfully predict this flow. One very recent source of information on this issue is a highly resolved LES performed by Krajnovic and Davidson [2] for the present body, but at a Reynolds number four times lower than the real value. The principal observation of interest here is that no flapping of the type described above was observed. Yet, the *relative* turbulence levels in the separated shear layer were as high as in the experimental configuration. Excluding, probably minor, Reynolds-number effects and the possibility that flapping has a very long time scale exceeding the total simulation period, it thus appears that the turbulence level in the separated shear layer is related to stochastic processes (not excluding, of course, dynamic effects associated with large-scale, though turbulent, motion). Hence, it seems conceivable that RANS methods could capture the processes at issue.

An indication of the ability of the models to reproduce the turbulence level in the flow above the slanted surface is given in Fig. 5. This shows contours of turbulence energy at the same streamwise positions as the velocity fields in Fig. 4. Perhaps the most important position is the first, x/H=-0.305. All models seriously underpredict the level of turbulence energy,

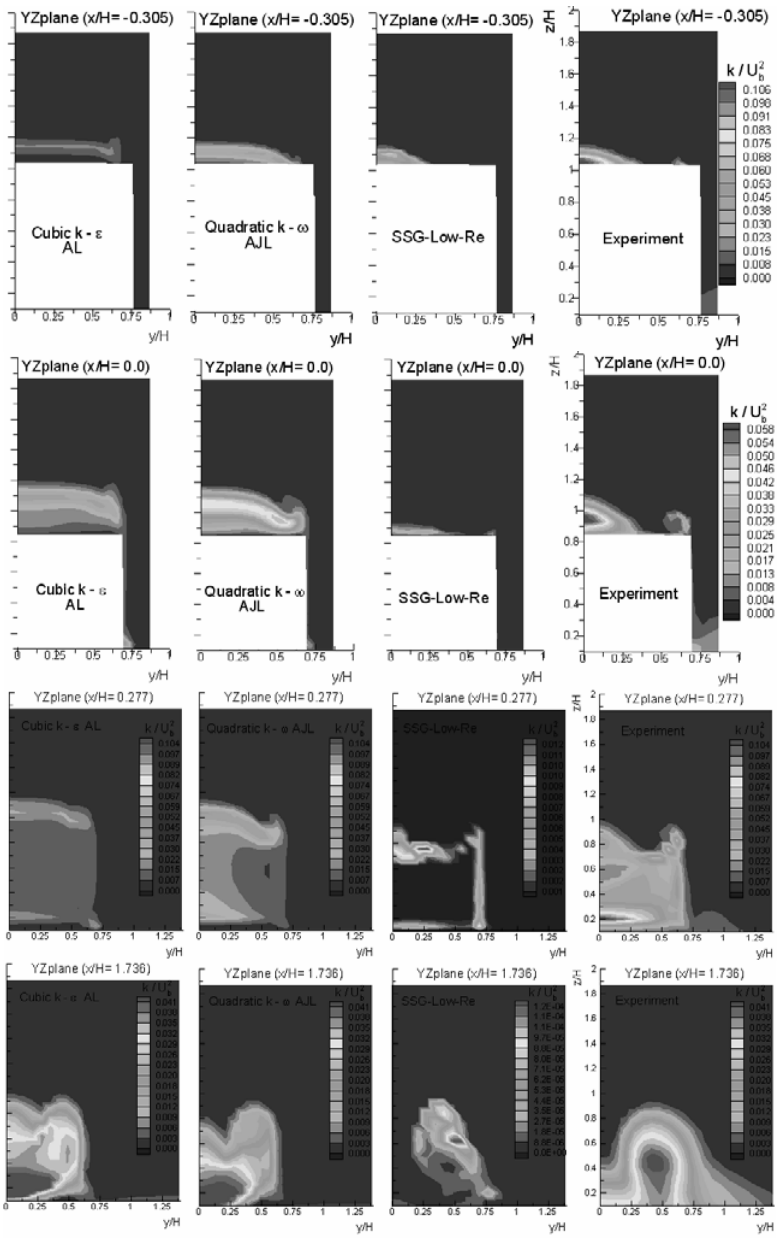

Fig. 5. Turbulence-energy fields in the y-z planes above the slanted surface and behind the body.

a defect observed earlier in 2-d conditions by Jang et al. [17]. However, the RSTM at least returns the correct region of elevated turbulence energy and a value which, while too low, is around 50% of that measured. The NLEVMs give much lower levels and hence fail to cause the flow to recover from separation. At *x/H*=0, both the real flow and that predicted by the RSTM are reattached. The calculation produces a low level of turbulence, due mainly to the inhibiting effect of the wall, while the experimental flow is highly disturbed by large-scale motions (i.e., dynamics) which maintain the boundary layer in a much more agitated state than can be reproduced by any of the turbulence models. Finally, in the free wake, it is the NLEVMs which do best, but for the wrong reasons. In this region, the models predict a much too intense recirculation and shear, thus causing excessive levels of turbulence.

5. Conclusions

Flow separation from any three-dimensional body represents a major challenge to any computational procedure. This is especially so in an asymmetric bluff body in which the flow is effectively very close to a separation/attachment 'cusp'. In the present case, the ability of the predictive models to resolve the separation process is evidently the key to achieving a credible representation of the flow as a whole and in the wake of the body, in particular. This separation dictates the lift on the body and thus the shed vortices and the transverse rotational motion in the wake. Given the bluff-body geometry, the presence of large-scale unsteady features in the wake must be expected. These may or may not include a non-stochastic, organized component. In any event, the large-scale unsteady motion in the wake will necessarily feed back to the separation region immediately around the slanted surface and is thus likely to induce a highly unsteady separation behavior. The dynamics of this process can obviously not be captured by any steady RANS scheme. For this reason, considerable caution is called for in making any categorical statements on the predictions presented in this paper. However, because RANS is still the dominant mode of predicting most practical flows, it is entirely defensible to examine the performance of alternative RANS closures for this difficult case and derive indications on characteristic predictive differences.

An important conclusion derived from the study is that the non-linear eddy-viscosity models examined do not constitute, for this flow, a credible approach to resolving the separation process. The main problem is that they return a far too low level of turbulence activity in the separated shear layer, so that the flow, once separated, does not reattach. As a consequence, the pressure field on the slanted surface is seriously at odds with reality, and the side vortices tend to be suppressed, reflecting far too weak lift and circulation. A second, related, conclusion is that a model that is able to capture, for whatever reason, the reattachment of the separated shear layer emanating from the roof will also predict broadly correctly the formation of the side vortices. Although the Reynolds-stress model does not give a satisfactory representation of the flow details, it *is* able to capture the reattachment on the slanted surface, thus also reproducing the rotational transverse motion well. An important question that must remain open is why precisely it is able to do so. The results for the turbulence energy show that this model also predicts a substantially too low level of turbulence energy in the shear layer above the slanted surface. Evidently, however, the shear-stress field is such that the shear layer is able to reattach. Whether the physical processes responsible for this reattachment are correctly reproduced by the model remains uncertain at this stage.

References

[1] C. Hinterberger, M. García-Villalba and W. Rodi, LES of flow around the Ahmed body. Lecture notes in applied mechanics, Proceedings of the UEF conference on The Aerodynamics of Heavy Vehicles: Trucks, Busses and Trains, Monterey/CA 2002 (to be published 2003, Springer Verlag) (2002).

[2] S. Krajnovic and L. Davidson, Large eddy simulation of the flow around a simplified car model, SAE 2004 World Congress, SAE Paper 2004-01-0227, Detroit, Michigan, USA. (2004).

[3] H. Lienhart and S. Becker, Flow and turbulence structure in the wake of a simplified car model. SAE Technical Paper 2003-01-0656 (2003).

[4] S. R. Ahmed, G. Ramm and G. Faltin, Some salient features of the time-averaged ground vehicle wake, SAE Technical paper 840300 (1984).

[5] R. Manceau and J.-P. Bonnet (Eds). CASE 9.2: Periodic flow over a 2-D hill. Proc. 10th ERCOFTAC (SIG-15)/IAHR /QNET-CFD workshop on Refined Turbulence Modelling, October 10-11, University of Poitiers, France (2002).

[6] F.-S. Lien and M.A. Leschziner, A General non-orthogonal collocated finite volume algorithm for turbulent flow at all speeds incorporating second-moment turbulence-transport closure, Part I: Computational implementation. Comput. *Methods Appl. Mech. Engrg.*, 114 (1994) 123-148.

[7] D. D. Apsley and M. A. Leschziner, Investigation of advanced turbulence models for the flow in a generic wing-body junction. *Flow, Turbulence and Combustion*, 67 (2001) 25-55.

[8] F.-S. Lien and M.A. Leschziner, Upstream monotonic interpolation for scalar transport with application to complex turbulent flows. *Int. J. Num. Meths. in Fluids*, 19 (1994) 527-548.

[9] D. D. Apsley and M. A. Leschziner, A new low-Reynolds-number non-linear two- equation turbulence model for complex flows. *Int. J. Heat and Fluid Flow,* 19 (1998) 209-222.

[10] K. Abe, Y.-J. Jang and M. A. Leschziner, An investigation of wall-anisotropy expressions and length-scale equations for non-linear eddy-viscosity models. *Int. J. Heat and Fluid Flow,* 24 (2003) 181-198.

[11] C. G. Speziale, S. Sarkar and T. B. Gatski, Modelling the pressure-strain correlation of turbulence: an invariant dynamical systems approach. *Journal of Fluid Mech*., 227 (1991) 245-272.

[12] H. C. Chen, Y.-J. Jang and J. C. Han, Computation of heat transfer in rotating two-pass square channels by a second-moment closure model. *Int. J. Heat and Mass Transfer,* 43 (2000) 1603-1616.

[13] B. E. Launder and B. I. Sharma, Application of the energy–dissipation model of turbulence to the calculation of flow near a spinning disc*, Lett. Heat Mass Transfer*, 1 (1974) 131-138.

[14] D. C. Wilcox, Simulation of transition with a two-equation turbulence model, *AIAA Journal*, 32 (1994) 247-255.

[15] W. Rodi, A new algebraic relation for calculating the Reynolds stresses, *Z. Angew. Math. Mech*., 56 (1978) 219-221.

[16] T. B. Gatski and C. G. Speziale, On explicit algebraic stress models for complex turbulent flows, *Journal of Fluid Mech.*, 254 (1993) 59-78.

[17] Y.-J. Jang, M. A. Leschziner, K. Abe and L. Temmerman, Investigation of anisotropy- resolving turbulence models by reference to highly-resolved LES data for separated flows. *Flow, Turbulence and Combustion,* 69 (2002) 161-203.

[18] D. D. Apsley and M. A. Leschziner, Advanced turbulence modelling of separated flow in a diffuser. *Flow, Turbulence and Combustion,* 63 (1999) 81-112.